Whole organ volumetric sensing Ultrasound Localization Microscopy for characterization of kidney structure

Georges Chabouh, Louise Denis, Sylvain Bodard, Franck Lager, Gilles Renault, Arthur Chavignon, Olivier Couture

Whole organ volumetric sensing Ultrasound Localization Microscopy for characterization of kidney structure

Georges Chabouh, *Member, IEEE*, Louise Denis *Member, IEEE*, Sylvain Bodard *Member, IEEE*, Franck Lager, Gilles Renault, Arthur Chavignon *Member, IEEE* and Olivier Couture *Senior member, IEEE*

***Abstract*— Glomeruli are the filtration units of the kidney and their function relies heavily on their microcirculation. Despite its obvious diagnostic importance, an accurate estimation of blood flow in the capillary bundle within glomeruli defies the resolution of conventional imaging modalities. Ultrasound Localization Microscopy (ULM) has demonstrated its ability to image in-vivo deep organs in the body. Recently, the concept of sensing ULM or sULM was introduced to classify individual microbubble behavior based on the expected physiological conditions at the micrometric scale. In the kidney of both rats and humans, it revealed glomerular structures in 2D but was severely limited by planar projection. In this work, we aim to extend sULM in 3D to image the whole organ and in order to perform an accurate characterization of the entire kidney structure. The extension of sULM into the 3D domain combined with a 3D subwavelength motion correction algorithm allow better localization and more robust tracking. The 3D metrics of velocity and pathway angular shift made glomerular mask possible. This approach facilitated the quantification of glomerular physiological parameter such as an interior traveled distance of approximately 7.5 ± 0.6 microns within the glomerulus. This study introduces a technique that characterize the kidney ~~phisiology~~physiology which can serve as a method to facilite pathology assessment. Furthermore, its potential for clinical relevance could serve as a bridge between research and practical application, leading to innovative diagnostics and improved patient care. .**

***Index Terms*— Sensing Ultrasound Localization Microscopy, 3D Super-resolution echography, kidney, glomeruli, medulla, vasa-recta, microbubbles.**

I. Introduction

GLOMERULI represent the filtration units of the kidney. In clinical practice, the change in the estimated glomerular filtration rate (GFR) - measured by blood or urine tests - is directly related to the degree of renal dysfunction [1]. In fact glomerular diseases represents the highest impact on kidney allograft loss [32]. In contrast to laboratory measurements, imaging enables direct visualization and quantification of kidney tissue remodeling, inflammation, and fibrosis [2]. However, accurately estimating blood flow at the scale of tenths of a millimeter within glomeruli defies the resolution capabilities of conventional ultrasound, computed tomography (CT), and magnetic resonance imaging (MRI) [3].

Ultrasound Localization Microscopy (ULM) has demonstrated its capacity to image in-vivo deep organs in the body [4]–[6], including the human renal graft [7], brain [13] and various human organs in 2D such as the liver and the kidney [48]. It has emerged as a powerful technique that has successfully overcome the limitations imposed by the diffraction barrier, enabling the acquisition of high-resolution images in-vivo. The technology has demonstrated its potential for imaging the microcirculation in various organs such as brain [33], spinal cord [34] and for healthy [26], [41] and diseased kidney [46], [47] in 2D and in 3D [50] in rodents. To harness ULM's clinical benefits, we must integrate it into routine medical practice and establish new biomarkers. Beyond the mere attainment of exquisite images, there exists the pressing need to explore and exploit ULM's capabilities for advanced medical analyses, such as the estimation of blood volume and other relevant clinical features as discussed in a recent review [35]. Therefore, the current focus should shift towards harnessing ULM's potential as a versatile tool for quantitative and functional assessments, paving the way for its practical implementation in clinical settings. Various research studies goes into this direction such as using the vascular properties to study obesity through the kidney [23], or for functional [36] and dynamical imaging [37] of the brain or to study human breast cancer [49].

In a recent study [8], we introduced the concept of sensing Ultrasound Localization Microscopy (sULM) in 2D, revealing the kidney's functional structures (glomeruli) in both rats and humans grafts. By dividing the data into two categories of velocity: slow microbubbles in the medulla and glomeruli and fast ones in the bigger arteries, all kidney regions were characterized using specific metrics relying on the kinetics of these microbubbles.

However, a significant constraint in studying intrinsic microbubble behavior stemmed from the presence of vessels

"This work was supported in part by the European Research Council (ERC) through the H2020 Program (ERC Cog ResolveStroke 772786."

G. Chabouh, L. Denis, S. Bodard, A. Chavignon and O. Couture are in Laboratoire d'Imagerie Biomédicale, Sorbonne University, CNRS, INSERM, Paris, France (e-mail: georges.chabouh@sorbonne-universite.fr, louise.denis@sorbonne-universite.fr, sylvain.bodard@sorbonne-universite.fr, arthur.chavignon@sorbonne-universite.fr and olivier.couture@sorbonne-universite.fr)

F. Lager and G. Renault are in Institut COCHIN, CNRS, INSERM, Université Paris Cité, Paris, France. G.C and L.D contributed equally

running transverse to the imaging plane. As the microbubble deviates from the 2D imaging plane, its intensity progressively diminishes until it vanishes. This hinders the continuous tracking of the microbubble throughout its intravascular course. Moreover, relying on a lone 2D imaging plane restricts the potential diagnostic capabilities of sULM. While a conceivable solution involves multi-plane imaging, acquisition time becomes important [15]. Conversely, accurate quantification are hindered through 2D projections. Thus, a comprehensive solution lies in whole-organ 3D imaging, which not only addresses the aforementioned issues but also diminishes the requirement for user interpretation and manual probe placement.

In a recent work, 3D transcranial ULM was proposed as a discriminator between ischemic and hemorrhagic stroke in early phase for a preclinical model [21]. Various studies, propose a shift from qualitative imaging methods to a more quantitative approach. In fact, ULM was also used to study vasodilatation [38], [39], [45] in the brain as well as in the heart [40] both in pre-clinical studies.

In the presented work, our objective is to demonstrate that the implementation of 3D sULM enables accurate tracking of microbubble pathways throughout the entire intravascular trajectory. Additionally, we emphasize the capability of 3D sULM to achieve precise quantification of various physiological parameters, including factors like glomerular blood flow and size, working towards a more accurate estimation of the glomerular filtration rate (eGFR).

II. Materials and Methods

A. In-vivo rat model

All animal experiments were performed in accordance with the ARRIVE guidelines and approved by the local ethics committee (ethics committee on animal experimentation n°034). The protocol is registered by the ministry of research under number #33913-2021082311153607. In accordance with the 3R rules, the number of animals in our study was kept to the necessary minimum. Experiments were performed on 8 Wistar male rats (Janvier Labs, Charles River, Envigo) aged between 8 and 12 weeks. Only 5 rats were included due to technical problem with data acquisitions and saving. All 8 rats were used to set-up and validate the micro-CT terminal perfusion of baryum sulfate solution. Also, they allowed the realization of a complete 3D sULM mapping. Rats were anesthetized during the entire experiment (4% Isoflurane) and maintained at a temperature of 37°C using a heating table. The animals died during the injection of the micro-CT contrast medium detailed later in this section.

B. Ultrasound acquisitions

To perform the ultrasound acquisition, the left kidney was externalized through an incision in the abdomen (See Fig.1 **a**). The organ was then placed on an acoustic absorber and fixed with a needle to avoid movement. A 25G catheter was placed in the tail vein to perform microbubbles injections (SonoVue, Bracco, Italy) needed for volumetric sULM. The animal was

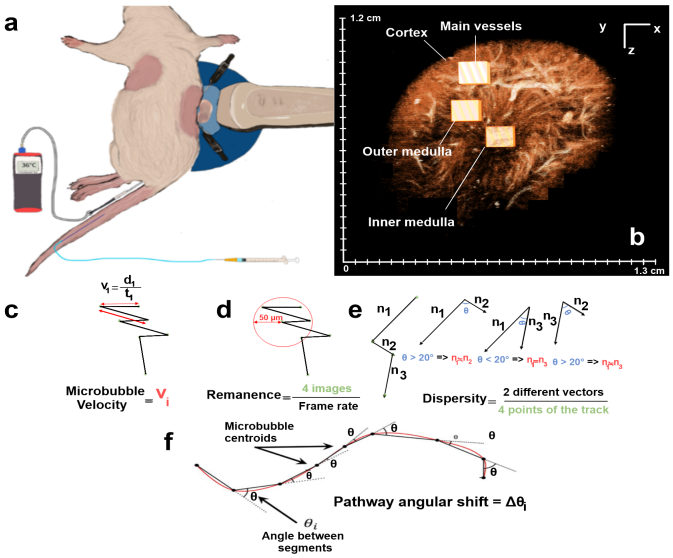

Fig. 1. Graphical methods: **a** In vivo setup of the rat kidney **b** 3D ROI of different renal zones were selected from sULM rendering. Representative cubes were chosen for each renal zone on the 3D density mapping and three different metrics used in this study: **c** normalized velocity, **d** Remanence and **e** the pathway angular shift is characterized as the difference between two successive angles, as derived and modified from [18]. Note that PAS does not account for distance normalization between the initial and final points.

under isoflurane anesthesia (4% for induction, 2.5% for maintenance) with appropriate analgesia (subcutaneous injection of 0.1 mg/Kg of buprenorphine 30 minutes prior to experiments).

Ultrasound acquisitions were then performed with a 256-channels research ultrasound scanner (verasonics, Kirkland, USA) and an 8 MHz multiplexed matrix probe (Vermon, France). Five hundred blocks were acquired, with 200 images per block and a framerate of 130Hz. Each image being the result of a compounding of 5 plane waves oriented according to $\pm$ 5° (in the elevation axis and in the lateral axis). ~~The sequence was decomposed according to a *light* configuration [9], and lasted for 8 minutes, with repeated bolus injections of 50 μL/min every 1 minute.~~ The multiplexed probe is divided into 4 panels of 256 elements each. The sequence used here uses a so-called "light" configuration, i.e. 10 shots per angle, corresponding to a transmission with one panel and a reception with its neighboring panels [9]. The sequence lasted for 8 minutes, with repeated bolus injections of 50 μL/min every 1 minute. The pulse duration is about 2 cycles with a pulse repetition frequency (PRF) of 13.5 kHz. The data were then reconstructed with a classical delay and sum beamforming [19] on a [98.5, 150, 150] μm grid, before reaching the final sULM resolution of [9.85, 9.85, 9.85] μm [20], [29].

C. Micro computed tomography (micro-CT) acquisitions

Micro-CT data were acquired on the same rats as the ones subjected to ultrasound acquisition at the Live Imaging Platform of the Odontology UFR Montrouge, France (Skyscan 1172, Bruker, [5, 5, 5] μm).

The X-ray opaque contrast medium consists of a mixture of barium sulfate (Micropaque 100 g, Guerbet, France),

PBS (Phosphate Buffer Saline, Cochin INSERM U1016), and gelatin. It was injected at the end of the ultrasound acquisitions through an aortic catheterization. All of the animal's blood was replaced by the contrast medium, i.e., approximately 200 mL/animal. The organ was then stored in a Petri dish for 48 h in 4% of PFA before being scanned in the micro-CT system described above.

Only 4 rats have usable micro-CT data due to the complex nature of the contrast agent injection [8], [10] procedure and the high risk of animal mortality during the process.

No statistical analysis was performed to compare sULM and micro-CT due to non-rigid deformations. Simply the manual registration on the AMIRA (Thermofischer, USA) software, allowed a descriptive assessment in 1 rat, i.e. the rat with the micro-CT and the most complete 3D sULM possible (see Fig.8).

D. Whole organ volumetric sULM

The construction pipeline of the 3D sULM mapping is shown in Fig.2. First, classical ultrasound compounded B-Mode volumes are acquired (Fig.2 **a**).~~In Fig.2 **a** classical ultrasound Bmode volume reconstruction,~~ Fig.2 **b** shows the clutter filtering using a low-threshold ~~Singular Value Decomposition~~ singular value decomposition (SVD) where the first six singular values were annulled, this value is empirically-determined and set for all rats. The detection was made using a local maximum on 900 MBs/volume with a local signal to noise ratio (SNR) value of 9. **c** highlights the microbubble localization step using radial symmetry algorithm [11], [12], and **d** shows the tracking step using the Hungarian algorithm [14] with a maximum linking distance of 2.3 voxel. It is worth to mention that in this work, the localization and tracking were done on an unique dataset. Contrary to 2D sULM [8], where the dataset was divided into two sup-groups: fast moving microbubbles and slow moving microbubbles. Thanks to the volumetric acquisition, we were able to precisely track the microbubble along its entire path within the blood vessels without any loss of visual continuity without the need of separating dataset. One explanation comes from the natural sparsity of microbubble data in 3D, making localization and tracking more feasible and another reason is a better matching between pairs of localization under constraints of maximum linking distance.

E. 3D ROI in different renal zones

An arbitrary 3D region of interest (ROI) was delineated within the four principal regions of the kidney: main vessels, inner medulla, outer medulla, and cortex, as depicted in Fig.1 **b**. The ROIs were defined as cubic structures measuring 100 pixels on each side, corresponding to a size of 985 μm. Note that the cortical ROI is not seen from this angle.

F. 3D sULM metrics

sULM is built upon an a-priori knowledge of the local environment based on previous invasive microscopy studies such as histology [17]. To highlight specific microbubble behaviour, we employed two different metrics that we define hereafter.

- Microbubble *velocity*: characterized as the mean displacement magnitude between every two successive points along a trajectory, divided by the corresponding time interval (Fig.1 **c**).
- The *Remanence Time* : established as the maximum period during which a microbubble was tracked within a glomerular sphere, i.e. of 50 μm radius in the rat [16], [17]. The center was defined as the median of the list of points constituting the track (Fig.1 **d**).
- The *Dispersity*: corresponded to the number of times a track went in the same direction, by taking the rounded value of the location, with a tolerance of plus or minus 20°, divided by the number of points making up the track (Fig.1 **e**).
- The *Pathway Angular Shift (PAS)*: delineated as the angular difference computed between sets of three consecutive points along a track. To illustrate, envision a track consisting of ten points. The initial trio of points yields two lines, from which an angle can be derived. Subsequently, the subsequent three points generate another pair of lines, yielding a second angle. The disparity between these two angles defines the PAS ((Fig.1 **f**).)

G. Statistical analysis

Statistical analyses were performed to evaluate the metrics between the different regions of the kidney using a two-tailed parametric unpaired Student's t test with GraphPad Prism 9 software. The significance of the results is as follows: $ns = P \geq 0.05$, $* = P \leq 0.05$, $** = P \leq 0.01$, $*** = P \leq 0.001$, $**** = P \leq 0.0001$. All the metrics were calculated inside the above mentioned 3D ROIs as seen in Fig.1 **b** and averaged on 5 different rats ($n = 5$ included).

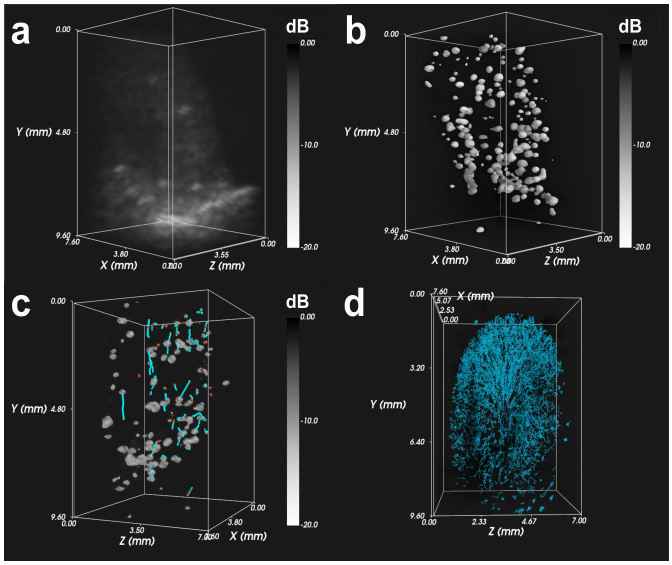

Fig. 2. 3D sULM steps: **a** B Mode, **b** tissue filtering, **c** microbubble localization and tracking, **d** tracks accumulation.

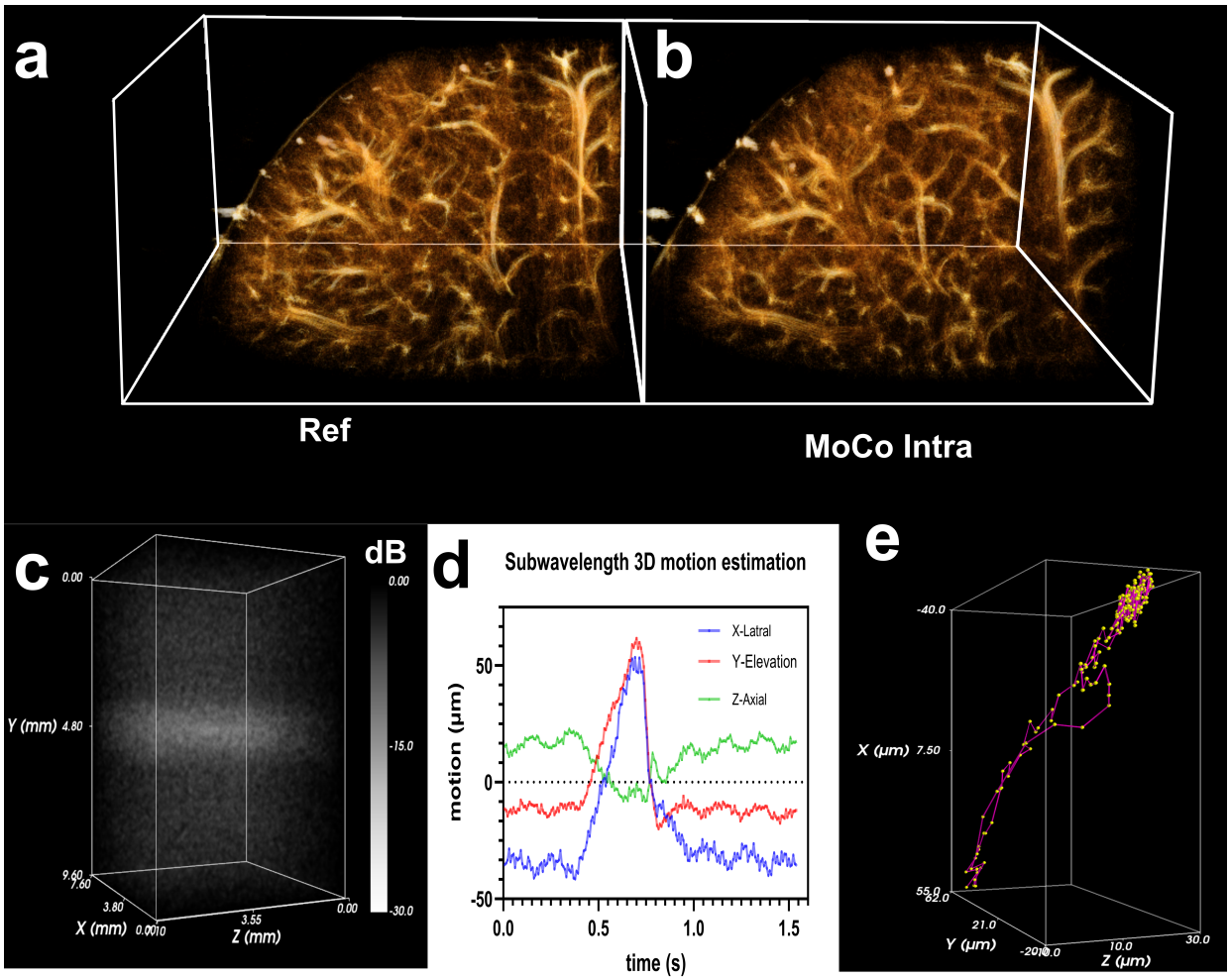

Fig. 3. 3D intra-bloc subwavelength motion correction: **a** 3D ULM reference image without motion correction **b** 3D ULM reference image with the proposed 3D motion correction **c** volumetric phase correlation between a reference frame and a given frame intra-bloc **d** Subwavelength motion estimation in the lateral, elevational and axial direction and **e** 3D trajectory of the displacement within one bloc (200 frames).

H. 3D subwavelength rigid motion correction

Motion induced by breathing, heartbeat and muscle contraction are usually higher than the micrometric scale of ULM ($\sim$ 10 μm). Hence, the estimation of tissue motion and the compensation play a crucial role for the quantification significance in ULM. Various motion compensation techniques has been applied for ULM such as speckle tracking [25] to correct for full deformation, two-stage motion correction that account for non-rigid and rigid deformation [42]. Lagrangian beamformer [27] was developed based on non-rigid motion registration to form images directly in the myocardium's material coordinates. ~~Yet, motion correction for volumetric ULM remains challenging.~~ In our study, we introduce ~~an innovative~~ a 3D subwavelength rigid motion correction method that utilizes phase correlation, a technique that has previously demonstrated its effectiveness in improving ULM resolution in 2D [28]. Briefly, inside a bloc of 200 frames (intra-bloc) the phase correlation is computed between a given ~~Bmode~~ B-Mode volume and a reference ~~BMode~~ B-Mode volume which is chosen to be central volume (i.e. frame = 100) as depicted in Fig.3 **c**. The inverse Fourier transform of the phase correlation is a Dirac peak in $[\Delta x \Delta y \Delta z]$. The intra-bloc motion is thus estimated in the lateral, elevational and axial dimensions (Fig.3 **e**) and its 3D trajectory is shown in **d**. The proposed 3D subwavelength motion compensation intra-bloc shows a significant improvement in the final image resolution (**b** compared to the reference image without motion correction **a**).

III. Results & Discussion

A. Vascular mapping along the entire microbubble path

The ~~relatively high~~ sufficient volumetric frame rate of our ultrasound acquisitions, enabled us to follow the microbubbles throughout their intravascular journey. Thanks to a single filter and a single tracking algorithm, a complete 3D mapping of the entire kidney in 5 rats was established. We sucessfuly observed the particularities of the microcirculation in each of the regions of the kidney (rat 8 in Fig.4 **a**, and **b**). In the main vessels, the microbubbles move very fast and are subdivided into interlobar arteries, arcuate arteries. The return path has also been reconstructed into an efferent arteriole, arched and interlobar veins In the cortex, some microbubbles ascend in the afferent artery, swirl in the glomerulus before returning to the cortex. We were also able to follow the entire route

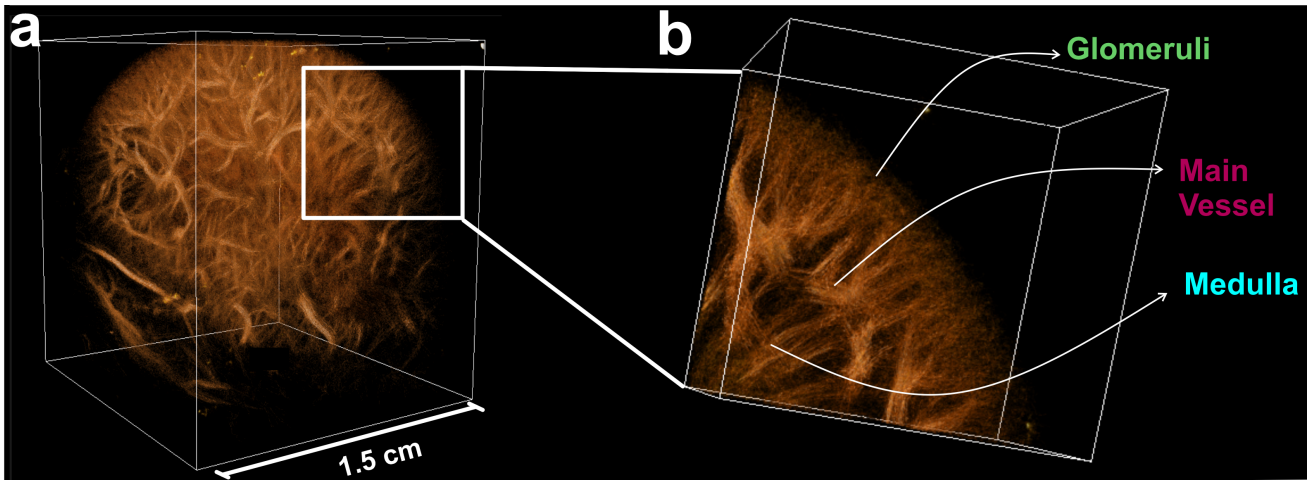

Fig. 4. **3D ULM mapping: a** Vascular mapping allows reconstruction of the entire volume of the kidney and **b** Zooming into the cortex allows observation of the renal functional units: the glomeruli

of the microbubble in the glomerulus. Finally, in the medulla, the microbubble path is less trivial but remains a characteristic of the renal physiology. The microbubbles appear to follow a straight path towards the center of the kidney, i.e. along the vasa recta at the level of the Malphigian pyramids. After a certain depth inside the inner medulla, a loss of visualisation of these microbubbles is remarked. This can be due to the limitation of the current spatiotemporal filter. In fact, the spatiotemporal based filter employed here might be unable to differentiate fixed or slow moving microbubbles from the tissue signal, since both are highly coherent in space and time. Moreover, the relatively short ultrasound block duration and the time delay between each block of the volumetric ultrasound acquisition present additional explanations for the reduced visualization of slow-moving microbubbles.

The main regions of the kidney can be easily distinguished through specific track features. In Fig.5, multiple individual tracks were manually chosen and displayed as a function of their velocity and the total distance traveled D_{Total}. All tracks are not on the same scale Four distinct track clusters are evident: green for glomeruli-like tracks, blue for medulla tracks, red for main vessel tracks, and black for outlayer tracks. Glomeruli-like tracks appear slender, forming bundles with spinning microbubbles. Medulla tracks are broader, displaying elongated yet sinuous trajectories. Main vessel tracks, even wider, remain straight. Velocity analysis distinguishes them: medulla tracks move slowly (1-5 mm/s), cortex tracks range from 5 to 10 mm/s, and main vessel tracks accelerate (10-15 mm/s). This observation of cortex velocity aligns with earlier research studies [43], [44]. Black outlayer tracks segment into two: high-velocity (12-14 mm/s) tracks cover short distances, possibly due to framerate limitations capturing swift flows. An intermediate-speed outlayer track that might represents a microbubble in the afferent artery, just entering the glomerula or another possible scenario. Remarkably, within the medulla, no track surpasses 0.1 mm in distance owing to its slow pace; the brief acquisition time restricts extended tracking. Lastly, it is notable that tracks within the medulla and the glomeruli can exhibit comparable speed and travel distance, posing a challenge for differentiation, as discussed further on.

B. 3D metrics to characterise the microcirculation

In order to characterize the kidney's microcirculation on a macroscopic scale accurately in 3D, we conducted a comparative analysis of metric values across various renal regions in rats. First, volumetric sULM *velocity* rendering is shown in Fig.6 **a**. Values ranging from 1 to 10 mm/s, the low speed corresponds to the tracks in the inner medulla and in the upper region of the cortex, intermediate speeds are more present in the arteries of the cortex and finally high speed dominate in the main vessels (interlobar and arcuate arteries). Two cross sections in the coronal and sagittal planes in **b** and **c** display the velocity values. Statistical analysis of the metrics were represented by boxplot topped by a Student's statistical test with a confidence level of 95% (Fig.6 **d**, **f** and **h**) and their spatial representation are displayed in Fig.6 **b**, **c**, **e** and **g**.

The boxplot in Fig.6 **d** shows that the *velocity* can be a good discriminater between the four regions of the kidney. The microflow speed is high in the main vessels and almost double the speed in the cortex while the latter is also double the speed in the medulla, the deeper the microbubble flows in the inner medula, the lower their velocity gets. No statistical significance in difference between the inner and outer medulla. Note that the speed in the main vessels should be in order of cm/s in rat's kidney [22] hence it is underestimated due to a volumetric imaging rate of 130 frame/s. The path of the microbubbles found in the medulla, whether internal or external, exhibit statistically slower, more dispersed, and more remanence compared to those present in the cortex (Fig.6 **f** and **h**). The difference with the values of the metrics between the cortex and the main vessels is statistically significant. For instance, the *remanence* in the cortex is around 10 frames while it is around 6 in the main vessels. Regarding the values of the metrics in the medulla and the glomeruli, they seem to be similar (Fig.6 **f** and **h**). The similarity is hardly surprising, given that both structures are composed of capillaries.

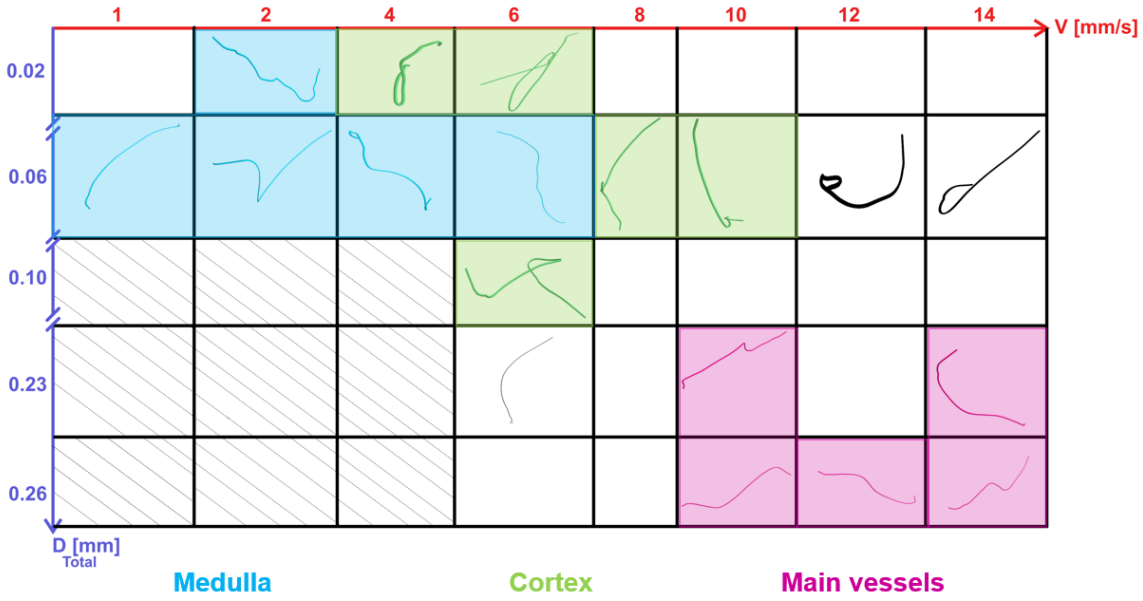

Fig. 5. **Ethology of 3D sULM tracks**: manually selected tracks from all the renal regions. Medullar tracks in light blue. Glomeruli-like tracks in green, Main vessel tracks in red and outlayer tracks in black. All volumetric views are centered on the tracks for displaying clarity, thus tracks do not have the same scale. The tracks are displayed regarding the average velocity on the red x-axis and the total traveled distance ion the ~~green~~ blue y-axis.

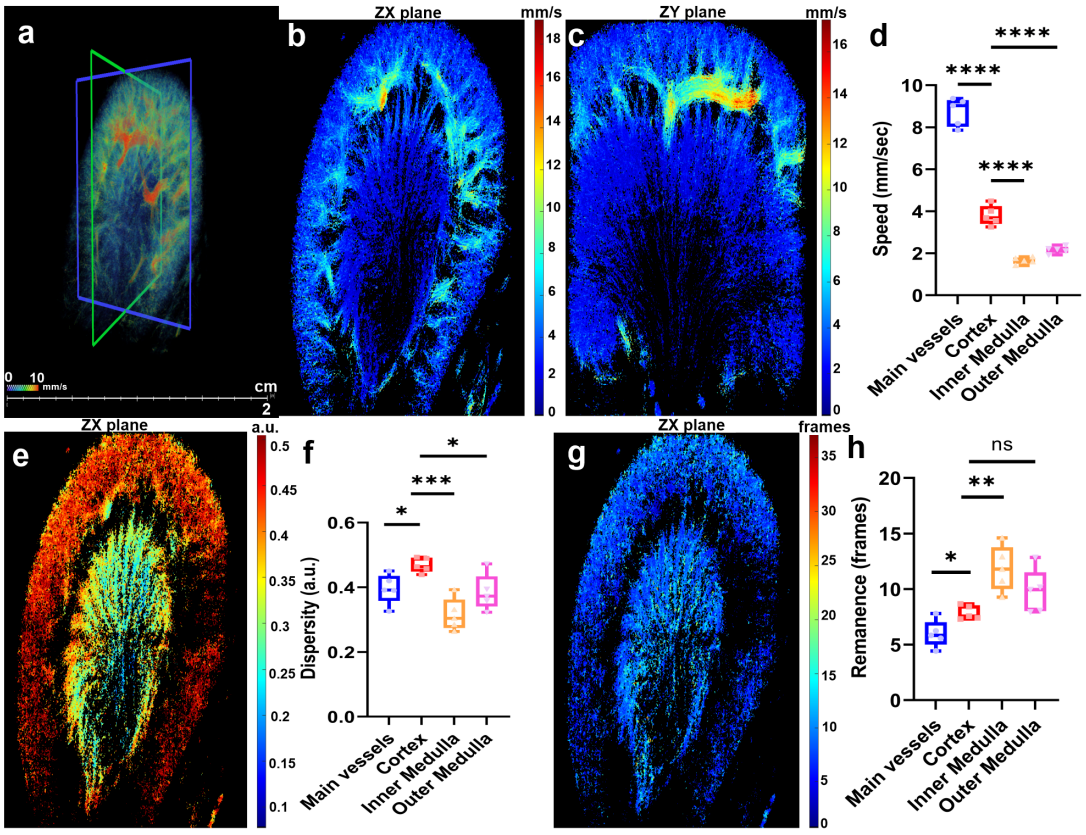

Fig. 6. **Comparison of the metrics within different renal regions: main vessels, cortex, inner medulla, and outer medulla. a** Volumetric velocity map. Velocities within the different regions in the coronal (blue) and sagittal (green) planes are shown in **b**, **c**. Boxplot for *velocity* estimation in **d**. *Dispersity* within the different regions **e** and its corresponding boxplot **f**. *Remanence* within the different regions, **g** and its corresponding boxplot **h**.

C. Glomeruli physiological estimation

To estimate physiological parameters like the glomerular filtration rate, it is essential to carefully pinpoint glomeruli within the cortex. This task is achieved through a systematic two-step approach: Firstly, cortical tracks are extracted by

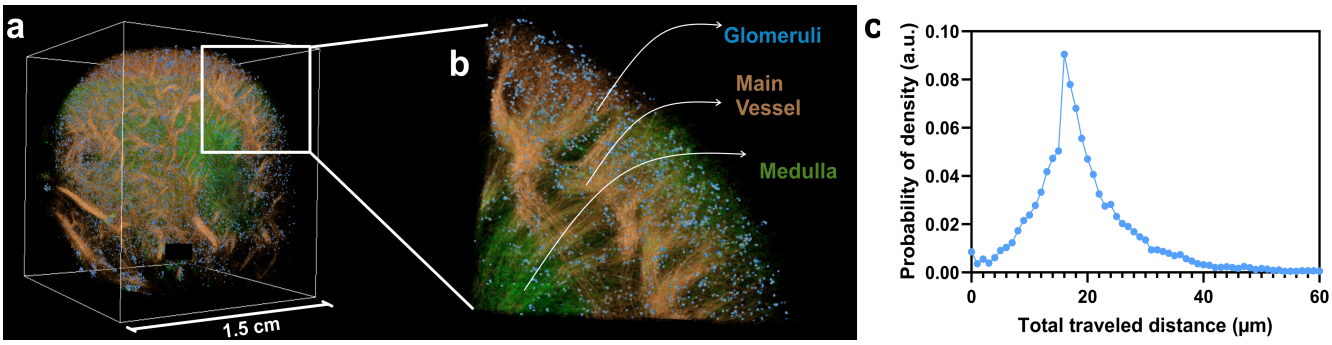

Fig. 7. **Whole organ volumetric sULM reveals accurate estimation of glomeruli physiology: a** Volumetric sULM rendering with three different families encoded in color. Medulla in green, main vessels in orange and glomeruli in blue. **b** shows a zoom on a part of the kidney. The probability of density of all the glomeruli tracks (in blue) of the total traveled distance i.e. the track length of the tracks counted as glomeruli **c**.

applying a velocity threshold ($3 <$ track speed < 6 mm/s) which is in agreement with the in-vivo measurement of [43], [44]. This velocity parameter serves as a discriminant, effectively distinguishing various segments of the kidney's structure (refer to Fig. 6 **d**). Subsequently, the Pathway Angular Shift (PAS) metric (outlined in Sec. II-F) is employed on the tracks established via the dual velocity cutoff. If the computed PAS value surpasses a designated threshold of 40 degrees, all data points exhibiting $PAS > 40°$ are identified as localizations within the glomerulus. Note that the threshold value used in PAS is empirical.

Figure 7 depicts the central findings of this study. In Fig.7**a**, 3D sULM rendering of the kidney is displayed, with a closer view provided in **b**. Note that the kidney view in Fig.7 **a** and **b** is the same as Fig.4. Here, glomeruli are highlighted in blue, main vessels in orange, and the medulla in green. In Fig. 7 **c** demonstrates the probability function for the total traveled distance, which reaches its peak at 18 μm. Notably, due to the complex presence of various vessel loops within the capsule, determining the size of the glomeruli through microcirculation is impractical. To approximate a size-related metric, we propose utilizing the total traveled distance within the glomeruli. Upon statistical analysis encompassing all the glomeruli across the rat population, a total traveled distance of 7.5 ± 0.6 μm is obtained. This measurement is notably smaller than the actual glomerular size (which boasts a 50-micron diameter).

D. Ex-vivo reference technique

The preparation of ex vivo specimens for micro-CT imaging is a crucial step that eliminates the influence of neural or chemical signals responsible for vessel constriction or dilation, thus affecting vessel proportions. Nevertheless, it's vital to acknowledge that the micro-CT imaging process itself can be invasive and may introduce significant artifacts while quantifying results. Factors such as tissue swelling, perfusion pressure during contrast administration, and the effects of contrast curing and paraffin embedding can complicate precise measurements of vessel dimensions. As a qualitative comparison, we observe identical microvascular structures for both techniques as seen in Fig. 8. However, as mentioned in [24], comparing in-vivo super-resolution ultrasound with ex-vivo microvascular imaging technique (micro-CT) becomes complex.

IV. Conclusions & Limitations

In this study, we proposed a whole organ ultrasound imaging technique. The utilisation of 3D sULM in rat kidneys allowed an accurate volume reconstruction of the microvascular mapping in 5 rats. The ~~high~~ sufficient volumetric rate of the acquisition and the low threshold of spatiotemporal filtering made it possible to follow the microbubbles along their intravascular with a single tracking algorithm. In this manner, we achieved a comprehensive examination of microbubble behavior within cappillaries such as in both the vasa recta of the medulla and the nephrons in the cortex. This work allowed us to witness, microbubbles circulating within the renal functional units in 3D, in-vivo, in the pre-clinical phase. Additionally, we could observe microbubbles in the medulla, a complex region that remains relatively understudied in nephrology. The vasa recta appears to be correctly reconstructed from the main vessels, and we were able to characterise it using 3D metrics. The use of metrics in each of the renal zones enabled us to compare the behaviour of microbubbles in the different structures of the kidney. Moreover, an innovative glomerular mask was adopted, uniting microflow velocity with the PAS. This straightforward method enables a precise quantitative evaluation of glomerular

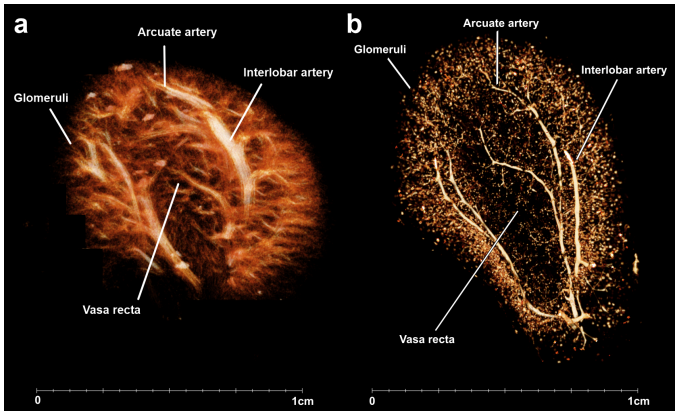

Fig. 8. Comparison of the main structures between 3D sULM and micro-CT imaging on the rat kidney. a) 3D sULM, b) Micro-CT.

physiological parameters—an important stride towards GFR estimation.

One of the main limitations of this study lies in the specificity of the metrics used for each of the applications. It would be important to test each metric under various conditions such as: pre-clinical and clinical settings, and evaluating performance across healthy organs and pathologies.

Another limitation stems from the absence of a readily applicable technique for direct comparison with 3D sULM's high resolution. Micro-CT imaging, the closest candidate, presents challenges due to its invasive nature, potentially causing discomfort to animals and consequently compromising contrast fixation.

Finally, the low-threshold spatiotemporal filtering allowed us to observe very slow flows in the cortex and medulla. Nevertheless, we observed a loss of signal from microbubbles in the center of the vasa recta (medulla). In our opinion, this decrease in intensity is due to the filtering, which considers the microbubble to be quasi-static and coherent (due to its high intensity), and therefore the microbubble signal and the tissue are indistinguishable entities during the process. The lack of precise localization could potentially result in pairing errors within the center of the medulla, creating a "blurred" effect in this region. However, since the medullary region is a relatively understudied capillary complex, this remains a hypothesis that requires further investigation and verification.

A. Perspectives

The emergence of 3D sULM as a promising technique brings about new possibilities. Its non-invasive, in-vivo characteristics provide distinct advantages. As we delve into optimizing the use of 3D sULM to gain deeper diagnostic insights into various pathologies, it's important to exercise caution and acknowledge the current limitations it carries. Important validation process involves ensuring its applicability across diverse biological systems and experimental conditions.

Extending the visualization duration of microbubbles is a critical aspect of 3D sULM. It effectively transforms them into mobile pressure sensors, enabling dynamic adaptation to various environments during their prolonged journeys. This augmentation in acquisition time empowers microbubbles to explore diverse conditions, yielding a richer trove of information. From a technological standpoint, this advancement relies on faster and more powerful hard disks, allowing continuous acquisitions without inter-block waiting times, and enhancing the capabilities of 3D sULM.

Additionally, faster computing capabilities would enable real-time processing and direct visualization of the acquired 3D sULM data. This feature would be invaluable for guiding imaging procedures, allowing researchers to verify the quality of the data as it is being acquired, and potentially making adjustments on-the-fly to optimize the imaging process.

Finally, to ensure accurate localization and tracking of both fast and slow microbubbles, there is a crucial need for more robust clutter filtering techniques. Deep learning-based filters, such as neural networks, offer promising solutions, harnessing their potential to effectively distinguish clutter from microbubble signals. Additionally, exploiting the non-linear properties of contrast agents [30], [31] combined with sULM can further enhance the filtering process.

APPENDICIES

ACKNOWLEDGMENT

We thank the "Live Imaging Platform" (Université de Paris-Cité), and specifically Lotfi Slimani for the micro-CT acquisitions with the Skyscan 1172 Bruker.

This study was funded by the European Research Council under the European Union Horizon 586 H2020 program/ERC Consolidator grant agreement No 772786-ResolveStroke.

O.C. holds patents in the field of ultrasound localization microscopy and is a cofounders and shareholders of the ResolveStroke startup.

REFERENCES

[1] M. Lenz, A. Harland, P. Egenolf, M. Horbach, C. von Hodenberg, P. Brinkkoetter, T. Benzing, P. Eysel and M.J. Scheyerer "Correlation between kidney function and mortality in pyogenic spondylodiscitis: the glomerular filtration rate (GFR) as new predictive parameter?," European Spine Journal, vol. 32, no. 4, pp. 1455-1462, Feb. 2023

[2] J. Kassirer, "Clinical evaluation of kidney function: Glomerular function," New England Journal of Medicine, vol. 285, no. 7, pp. 385-389, Aug. 1971

[3] M. Irazabal, L. Rangel, E. Bergstralh, S. Osborn, A. Harmon, J. Sundsbak, K. Bae, A. Chapman, J. Grantham, M. Mrug and others "Correlation between kidney function and mortality in pyogenic spondylodiscitis: the glomerular filtration rate (GFR) as new predictive parameter?," Journal of the American Society of Nephrology: JASN, vol. 26, no. 1, pp. 160, Feb. 2015

[4] C. Errico, J. Pierre, S. Pezet, Y. Desailly, Z Lenkei, O. Couture, M. Tanter, 'Ultrafast ultrasound localization microscopy for deep super-resolution vascular imaging," Nature, vol. 527, no. 7579, pp. 499-502, Nov. 2015

[5] K. Christensen-Jeffries, O. Couture, P. Dayton, Y. Eldar, K Hynynen, F. Kiessling, M. O'Reilly, GM. Pinton, G. Schmitz, Tang MX and others, 'Super-resolution ultrasound imaging," Ultrasound in medicine & biology, vol. 46, no. 4, pp. 865-891, April 2020

[6] O. Couture, V. Hingot, B. Heiles, P. Muleki-Seya, M. Tanter, 'Super-resolution ultrasound imaging," IEEE transactions on ultrasonics, ferroelectrics, and frequency control, vol. 65, no. 8, pp. 1304-1320, Aug. 2018

[7] S. Bodard, L. Denis, V. Hingot, A. Chavignon, A. Aissani, O. Heleon, D. Anglicheau, O. Couture and JM. Correas "Ultrasound localization microscopy of the human kidney allograft on a clinical ultrasound scanner," Kidney International, vol. 103 no. 5, pp. 930-935, May. 2023

[8] L. Denis, S. Bodard, V. Hingot, A. Chavignon, J. Battaglia, G. Renault, F. Lager, A. Aissani, O. Heleon, O. Couture and JM. Correas "Sensing ultrasound localization microscopy for the visualization of glomeruli in living rats and humans," Ebiomedicine, vol. 91, May. 2023

[9] A. Chavignon, B. Heiles, V. Hingot, C. Orset, D. Vivien and O. Couture "3D transcranial ultrasound localization microscopy in the rat brain with a multiplexed matrix probe," IEEE Trans on Biomedical Imaging, vol. 69, no. 7, pp. 2132-2142, Dec. 2021

[10] P. Blery, P. Pilet, A. Vanden-Bossche, A. Thery, J. Guicheux, Y. Amouriq, F. Espitalier, N. Mathieu, P. Weiss, "Vascular imaging with contrast agent in hard and soft tissues using microcomputed-tomography," Journal of Microscopy, vol. 262, no. 1, pp. 40-49, Nov. 2016

[11] B. Heiles, M. Correia, V. Hingot, M. Pernot, J. Provost, M. Tanter, O. Couture, "Ultrafast 3D ultrasound localization microscopy using a 32x32 matrix array," IEEE Transactions on Medical Imaging, vol. 38, no. 9, pp. 2005-2015, Sept. 2019

[12] B. Heiles, A. Chavignon, V. Hingot, P. Lopez, E. Teston, O. Couture, "Performance benchmarking of microbubble-localization algorithms for ultrasound localization microscopy," Nature Biomedical Engineering, vol. 6, no. 5, pp. 605-616, Sept. 2022

[13] C. Demené, J. Robin, A. Dizeux, B. Heiles, M. Pernot, M. Tanter, F. Perren,"Transcranial ultrafast ultrasound localization microscopy of brain vasculature in patients," Nature biomedical engineering, vol. 5, no. 3 pp. 219-228, Mar. 2021

[14] JY. Tinevez, N. Perry, J. Schindelin, GM. Hoopes, G. Reynolds, E. Laplantine, S. Bednarek, S. Shorte, K. Eliceiri "TrackMate: An open and extensible platform for single-particle tracking," Methods, vol. 115, pp. 80-90, Feb. 2017

[15] F. Lin, S. Shelton, D. Espíndola, J. Pojas, G. Pinton, P. Dayton, "3-D Ultrasound Localization Microscopy for Identifying Microvascular Morphology Features of Tumor Angiogenesis at a Resolution Beyond the Diffraction Limit of Conventional Ultrasound ," Theranostics, vol. 7.1, pp. 196-204, Jan. 2017

[16] E. Baldelomar, J. Beeman, K. Bennett, P. Dayton, "Measuring rat kidney glomerular number and size in vivo with MRI ," American Journal of Physiology-Renal Physiology, vol. 314.3, pp. F399-F406, Mar. 2018

[17] P. Kimmelstiel, C. Wilson,"Intercapillary lesions in the glomeruli of the kidney ," The American journal of pathology, vol. 12. no. 1, pp. 83, Jan. 1936

[18] M. Lowerison, N. Sekaran, W. Whang, Z. Dong, X. Chen, D. Llano, P. Song"Aging-related cerebral microvascular changes visualized using ultrasound localization microscopy in the living mouse ," Scientific reports, vol. 12. no. 1, pp. 619, Jan. 2022

[19] V. Perrot, M. Polichetti, F. Varray, D. Garcia"So you think you can DAS? A viewpoint on delay-and-sum beamforming ," Ultrasonics, vol. 111., pp. 106309, Mar. 2021

[20] V. Hingot, A. Chavignon, B. Heiles, O. Couture"Measuring image resolution in ultrasound localization microscopy," IEEE transactions on medical imaging, vol. 40., no.12, pp. 3812-3819, Dec. 2021

[21] A. Chavignon, V. Hingot, C. Orset, D. Vivien, O. Couture"3D transcranial ultrasound localization microscopy for discrimination between ischemic and hemorrhagic stroke in early phase," Scientific Reports, vol. 12., no.1, pp. 14607, Aug. 2022

[22] Y. Feng-yi, C. Wei-Hsiu,"Focused ultrasound-modulated glomerular ultrafiltration assessed by functional changes in renal arteries," PLoS One, vol. 8., no.1, pp. e54034, Jan. 2013

[23] S. Søgaard, S. Andersen, I. Taghavi, C. Hoyos, C. Christoffersen, K. Hansen, J. Jense, M. Nielsen, C.Sørensen"Super-resolution ultrasound imaging provides quantification of the renal cortical and medullary vasculature in obese zucker rats: A pilot study," PLoS One, vol. 12., no.7, pp. 1626, Jul. 2022

[24] S. Andersen, I. Taghavi, H. Kjer, S. Søgaard, C. Gundlach, V. Dahl, K. Hansen, M. Nielsen, A. Dahl, J. Jensen C. Sørensen"Evaluation of 2D super-resolution ultrasound imaging of the rat renal vasculature using ex vivo micro-computed tomography," Scientific reports, vol. 1., no.1, pp. 24335, Dec. 2021

[25] I. Taghavi, S. Andersen, C. Hoyos, M. Nielsen, C. Sorensen, J. Jensen "In vivo motion correction in super-resolution imaging of rat kidneys," IEEE TUFFC, vol. 68., no.10, pp. 3082-3093, Oct. 2021

[26] J. Foiret, H. Zhang, T. Ilovitsh, L. Mahakian, S. Tam, K. Ferrara "Ultrasound localization microscopy to image and assess microvasculature in a rat kidney," Scientific Reports, vol. 7., no.1, pp. 13 662:1-12, Oct. 2017

[27] P. Cormier, J. Porée, C. Bourquin, J. Provost "Dynamic myocardial ultrasound localization angiography," IEEE TMI, vol. 40., no.102, pp. 3379-3388, Nov. 2021

[28] V. Hingot, C. Errico, M. Tanter, O. Couture "Subwavelength motion-correction for ultrafast ultrasound localization microscopy," Ultrasonics, vol. 77., pp. 17-21, May. 2017

[29] V. Hingot, C. Errico, B. Heiles, L. Rahal, M. Tanter, O. Couture "Microvascular flow dictates the compromise between spatial resolution and acquisition time in Ultrasound Localization Microscopy," Scientific Reports, vol. 9., no.1, pp. 2456, Dec. 2019

[30] G. Chabouh, B. Dollet, C. Quilliet, G. Coupier"Spherical oscillations of encapsulated microbubbles: Effect of shell compressibility and anisotropy," Journal of the Acoustical Society of America, vol. 149., no.2, pp. 1240-1257, Feb. 2021

[31] G. Chabouh, B. van Elburg, M. Versluis, T. Segers, C. Quilliet, G. Coupier"Buckling of lipidic ultrasound contrast agents under quasi-static load," Philosophical Transactions of the Royal Society A, vol. 381., no.2244, pp. 20220025, Feb. 2023

[32] Z. M. El-Zoghby, M.D. Stegall, D.J. Lager, W.K. Kremers, H. Amer, J.M. Gloor, F.G. Cosio "Identifying specific causes of kidney allograft loss," American Journal of Transplantation, vol. 9., no.3, pp. 527-535, Feb. 2009

[33] M. Lowerison, N.V. Sekaran, Z. Zhang, Z. Dong, X. Chen, D. Llano, P. Song,"Aging-related cerebral microvascular changes visualized using ultrasound localization microscopy in the living mouse," Scientific reports, vol. 12., no.1, pp. 619, Jan. 2022

[34] J. Harmon, Z. Khaing, J. Hyde, C. Hofstetter, X. Chen, C. Tremblay-Darveau, M. Bruce,"Quantitative tissue perfusion imaging using nonlinear ultrasound localization microscopy," Scientific reports, vol. 12., no.1, pp. 21943, Dec. 2022

[35] P. Song, J. Rubin, M. Lowerison,"Super-resolution ultrasound microvascular imaging: Is it ready for clinical use?," Zeitschrift für Medizinische Physik, May. 2023

[36] N. Renaudin, C. Demené, A. Dizeux, N. Ialy-Radio, S. Pezet, M. Tanter,"Functional ultrasound localization microscopy reveals brain-wide neurovascular activity on a microscopic scale," Nature methods, vol. 19., no.8, pp. 1004-1012, Aug. 2022

[37] C. Bourquin, J. Porée, F. lESAGE,J. Provost,"In vivo pulsatility measurement of cerebral microcirculation in rodents using dynamic ultrasound localization microscopy," IEEE Transactions on Medical Imaging, vol. 41., no.4, pp. 782-792, Ap. 2022

[38] B. Heiles, "3D ultrasound localization microscopy," PhD thesis, PSL Research University, Dec. 2019

[39] B. Heiles, A. Chavignon, A. Bergel, V. Hingot, H. Serroune, D. Maresca, ...O. COuture "Volumetric ultrasound localization microscopy of the whole rat brain microvasculature," IEEE Open Journal of Ultrasonics, Ferroelectrics, and Frequency Control,, no.2, pp. 261-282, Oct. 2023

[40] O. Demeulenaere, Z. Sandoval, P. Mateo, A. Dizeux, O. Villemain, R. Gallet, B. Ghaleh,T. Deffieux, C.Deméné, M. Tanter and others "Coronary flow assessment using 3-dimensional ultrafast ultrasound localization microscopy," Cardiovascular Imaging, vol. 15., no.7, pp. 1193-1208, Jul. 2022

[41] k. Reimer, M. Toulemonde, J. Yan, M. Lerendegui, E. Stride, P. Weinverg, C. Dunsby, M.X. Tang,"Fast and selective super-resolution ultrasound in vivo with acoustically activated nanodroplets," IEEE Transactions on Medical Imaging, vol. 42., no.4, pp. 1056-1067, Nov. 2022

[42] S. Harput, K. Christensen-Jeffries, J. Brown, Y. Li, K. J. Williams, A. H. Davies, R. J. Eckersley, C. Dunsby, and M. Tang,,"Two-stage motion correction for superresolution ultrasound imaging in human lower limb," IEEE TUFFC, vol. 65., no.05, pp. 803-814, May. 2018

[43] Y. Ogasawara, K. Takehara, T. Yamamoto, R. Hashimoto, H. Nakamoto, F. Kajiya "Quantitative blood velocity mapping in glomerular capillaries by in vivo observation with an intravital videomicroscope," Methods of information in medicine, vol. 39., no.02, pp. 175-178, Feb. 2000

[44] J. Engbjerg, D. Sardella, L. Bordoni, F. Trepiccione, G. Capasso, L. Østergaard, G.G. Rhodes, R. Sandoval, T. Ring, B.Molitoris and others"The Distribution of Blood in Renal Glomerular Capillaries Is a New Physiological Parameter, Which Is Affected by Diabetes and ACE-inhibition," The FASEB Journal, vol. 33., no.s1, pp. 748-11, Nov. 2019

[45] Y. Wang, M. Lowerison, Q.You, B. Lin, D. Llano, P. Song,"Longitudinal Awake Imaging of Deep Mouse Brain Microvasculature with Super-resolution Ultrasound Localization Microscopy," bioRxiv, pp. 2023–09, Sept. 2023

[46] Q. Chen, J. Yu, B.Rush, S. Stocker, R. Tan, K. Kim,"Ultrasound super-resolution imaging provides a noninvasive assessment of renal microvasculature changes during mouse acute kidney injury," Kidney international, vol. 98., no.2, pp. 355-365, Aug. 2020

[47] H. Zhang, L. Huang, Y.Yang, L. Qiu, Q. Le, J. Liu, L. Qian, and J. Luo"Evaluation of Early Diabetic Kidney Disease Using Ultrasound Localization Microscopy: A Feasibility Study," Journal of Ultrasound in Medicine, April. 2023

[48] C. Huang, W. Zhang, P.Gong, U. Lok, S. Tang, T. Yin, W. Zhang, L. Zhu, M. Sang, P. Song and others"Super-resolution ultrasound localization microscopy based on a high frame-rate clinical ultrasound scanner: An in-human feasibility study," Physics in Medicine & Biology, vol. 66., no.8, pp. 08NT01, Sept. 2021

[49] T. Opacic, S. Dencks, B.Theek, M. Piepenbrock, D. Ackermann, A. Rix, T. Lammers, E. Stickeer, S. Delorme, G. Schmitz and others"Motion model ultrasound localization microscopy for preclinical and clinical multiparametric tumor characterization," Nature communications, vol. 9., no.1, pp. 1–13, Sept. 2018

[50] K. Riemer, Q. Tan, S. Morse, L. Bau, M. Toulemonde, J. Yan, J. Zhu, L. Zhu, B. Wang, L. Taylor and others"3D Acoustic Wave Sparsely Activated Localization Microscopy With Phase Change Contrast Agents," Investigative Radiology, pp. 10–1097, Sept. 2023